Journal of Applied Analysis and Computation
Volume 16, Number 3, June 2026, 1621–1642
Website:http://www.jaac-online.com
DOI:10.11948/20250185

A (Q,τ)-FRACTIONAL AGING MODEL WITH MEMORY EFFECTS AND ADAPTIVE HEALING DYNAMICS

Shaher Momani[1,2] and Rabha W. Ibrahim[3,†]

Abstract We propose a novel (q,τ)-fractional aging model that incorporates memory-dependent physiological decay and healing dynamics through a deformable time structure. The model generalizes classical aging laws by introducing a tunable fractional order α and deformation parameters q and τ, which control the depth and scale of biological memory. External interventions, modeled as healing inputs, are integrated via generalized Mittag-Leffler kernels to capture both cumulative and periodic therapeutic effects. Simulation results demonstrate that composite healing strategies significantly delay decline and improve physiological resilience. Parameter sensitivity analysis reveals that the model flexibly adapts to different aging profiles by adjusting memory and deformation parameters. Using synthetic data, we validate the model's fitting accuracy through numerical optimization, achieving high fidelity with low residual error. The key advantage of the (q,τ)-fractional approach lies in its ability to encode long-term memory effects and nonuniform biological time flow, enabling realistic modeling of aging phenomena beyond exponential decay. The framework is robust under noisy conditions and extensible to data-driven calibration, making it a powerful tool for biomedical aging analysis, intervention design, and longitudinal health forecasting.

Keywords (q,τ)-fractional calculus, Mittag-Leffler function, memory-driven aging, biological time deformation, healing dynamics, non-exponential decay, parameter fitting, composite therapies, physiological modeling, residual analysis.

MSC(2010) 26A33.

1. Introduction

Biological aging is a complex, nonlinear process involving gradual deterioration of physiological systems, accumulation of damage, and loss of adaptive capacity. Traditional models often treat aging as an exponential decay process governed by memoryless dynamics, such as the Gompertz or Weibull laws. While effective for population-level mortality modeling, these frameworks fall short in capturing individual memory effects, therapeutic recovery, sport and long-range physiological dependencies [1, 4, 7, 18]. To address these limitations, fractional calculus has emerged as a natural and powerful tool. Fractional differential equations (FDEs) extend classical models by incorporating non-integer order derivatives, thereby encoding memory and hereditary effects intrinsic to biological tissues and processes. Such models have been widely applied to viscoelasticity, anomalous diffusion, epidemiology, and aging-related degradation [2, 6, 9].

[†]The corresponding author.
[1]Department of Mathematics, The University of Jordan, Amman, Jordan
[2]Nonlinear Dynamics Research Center (NDRC), Ajman University, Ajman, UAE
[3]Information and Communication Technology Research Group, Scientific Research Center, Al-Ayen University, Thi-Qar, Nasiriyah 64001, Iraq
Email: s.momani@ajman.ac.ae(S. Momani), rabhaibrahim@yahoo.com(R. W. Ibrahim)

A typical fractional aging equation may take the form:

$$\mathcal{D}_t^{\alpha} A(t) = -\lambda A(t) + f(t),$$

where $\mathcal{D}_t^{\alpha}$ denotes a fractional derivative of order $0 < \alpha < 1$, $A(t)$ represents the physiological state, λ is the decay rate, and $f(t)$ models healing or repair input. The use of the Mittag-Leffler function as a natural solution kernel provides a generalization of exponential decay, exhibiting power-law tails and memory-sensitive recovery. Figure 1 illustrates the essential

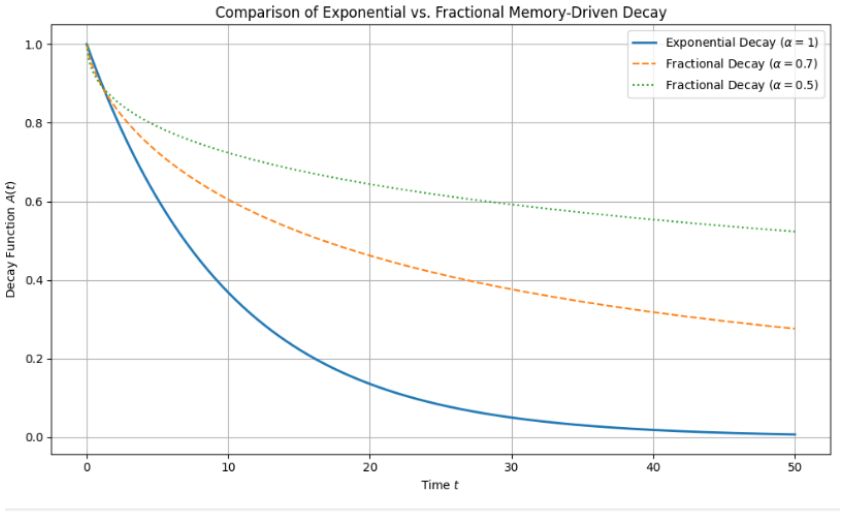

Figure 1. Comparison of exponential decay ($\alpha = 1$) and fractional memory-driven decay with $\alpha = 0.7$ and $\alpha = 0.5$. While the exponential model rapidly declines without memory, the fractional decay exhibits slower convergence, encoding long-term memory effects characteristic of biological systems.

difference between classical and fractional aging models. The exponential decay curve, which assumes no memory, decreases rapidly and uniformly. In contrast, the fractional curves governed by the Mittag-Leffler function exhibit a distinct long-tail behavior, leading to a slower decay over time. This memory effect reflects the biological reality that aging is not a Markovian process past states influence current dynamics. The parameter α controls the strength of memory: Lower α implies stronger memory and slower aging. This highlights the need for fractional-order models in applications involving tissue repair, chronic conditions, and long-term physiological degradation.

In this study, generalized FDEs incorporating deformed calculus [10, 11, 17] such as (q, τ)-fractional operators have been proposed to capture nonuniform biological time, fractal scaling, and adaptive processes [3, 12–15]. These operators modify both the time scale and the convolution structure, leading to enhanced flexibility in modeling diverse aging trajectories [5, 8, 16]. This work proposes a new aging model governed by a (q, τ)-fractional dynamic system, expressed as:

$$A(t) = A_0 E_{\alpha}^{(q,\tau)}\left(-\lambda (t)_{(q,\tau)}^{\alpha}\right) + \sum_{n=0}^{t-1} \left[(t-n)_{(q,\tau)}\right]^{\alpha-1} E_{\alpha,\alpha}^{(q,\tau)}\left(-\lambda (t-n)_{(q,\tau)}^{\alpha}\right) f(n),$$

where $E_{\alpha}^{(q,\tau)}(\cdot)$ denotes the (q, τ)-Mittag-Leffler function, and the time variable t is warped via a deformation mechanism depending on q and τ. This formulation allows us to model:

(i) Long-term memory and physiological inertia.

(ii) Composite healing strategies (e.g., periodic and exponential).

(iii) Biological time deformation and fractal-like decay behavior.

The remainder of the paper explores this model in detail, including simulations, parameter fitting, residual analysis, and validation using synthetic data. The goal is to provide a general-purpose, flexible modeling framework for capturing aging dynamics in biological and clinical contexts.

2. The (q,τ)-fractional calculus

Definition 2.1 ((q,τ)-Gamma function)**.** Let $z>0$, $0<q<1$, and $\tau>0$. The (q,τ)-Gamma function is defined as

$$\Gamma_{q,\tau}(z) := (1-q)^{1-z}\prod_{n=0}^{\infty}\frac{1-q^{\tau(n+1)}}{1-q^{\tau(n+z)}}, \quad \text{for } z\notin\mathbb{Z}_{\leq 0}=\{\dots,-3,-2,-1,0\}.$$

In the (q,τ)-fractional aging model, the parameters q and τ modulate the time memory kernel via the generalized deformation:

$$(t)_{q,\tau} := \frac{1-q^{\tau t}}{1-q}.$$

Here, $q\in(0,1)$ controls the degree of time compression, while $\tau>0$ scales the temporal deformation. Biologically, lower q values represent systems with extended memory and delayed response, such as in chronic aging or cumulative damage processes. Larger τ values induce nonlinear acceleration of aging, capturing phenomena such as early-stage degeneration or compressed biological time under stress. Together, q and τ allow for flexible, personalized modeling of physiological dynamics.

Remark 2.1. The (q,τ)-Gamma function generalizes the classical q-Gamma function by introducing a deformation parameter $\tau>0$ that governs the spacing of the base-q exponential terms. For $\tau=1$, one recovers the standard q-Gamma function $\Gamma_q(x)$.

Alternatively, in the discrete setting, it satisfies the recurrence:

$$\Gamma_{q,\tau}(z+1) = \left[(z)_{(q,\tau)}\right]\Gamma_{q,\tau}(z), \quad \Gamma_{q,\tau}(1)=1,$$

where

$$(z)_{(q,\tau)} := \frac{1-q^{\tau z}}{1-q^{\tau}}.$$

Figure 2 illustrates the behavior of the (q,τ)-Gamma function for a range of fractional deformation parameters. As expected, the function generalizes the classical Gamma curve, with increasing deformation for lower values of q and higher values of τ. When $q=0.9$ and $\tau=1$, the function closely resembles the classical $\Gamma(x)$, preserving its smooth growth and singularity near $x=0$. However, for $q=0.5$ and larger τ, the curve deviates significantly, flattening or growing faster depending on the range of x. This sensitivity to deformation parameters highlights the flexibility of $\Gamma_{q,\tau}(x)$ in modeling memory effects and scale transformations in fractional and nonlocal systems. These characteristics make it particularly suitable for memory kernels in climate health models and generalized dynamic systems.

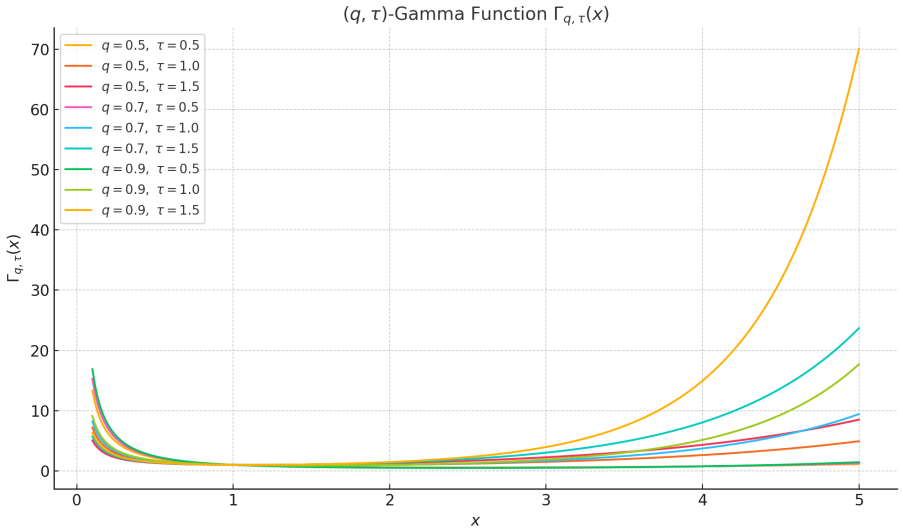

Figure 2. Plot of the (q,τ)-Gamma function $\Gamma_{q,\tau}(x)$ for various values of deformation parameters $q \in \{0.5, 0.7, 0.9\}$ and $\tau \in \{0.5, 1.0, 1.5\}$. The classical Gamma behavior is recovered as $q \to 1^-$ and $\tau \to 1$. For lower q, the function exhibits stronger deformation from the classical shape, especially as τ increases. These curves highlight how memory and scaling parameters affect growth and singularity behavior in fractional models.

Proposition 2.1 (Properties of the (q,τ)-Gamma function)**.** *Let $0 < q < 1$, $\tau > 0$, and $x > 0$. The (q,τ)-Gamma function satisfies the following properties:*

(i) Recursion:

$$\Gamma_{q,\tau}(x+1) = \frac{1-q^{\tau x}}{1-q}\Gamma_{q,\tau}(x).$$

(ii) Normalization: $\Gamma_{q,\tau}(1) = 1$.

(iii) Positivity: $\Gamma_{q,\tau}(x) > 0$ *for all* $x > 0$.

(iv) Asymptotic behavior: *For fixed τ, as $x \to \infty$,*

$$\Gamma_{q,\tau}(x) \sim C_{q,\tau} \cdot (1-q)^{1-x} q^{-\frac{1}{2}\tau x^2},$$

where $C_{q,\tau} > 0$ is a constant depending on q and τ.

Proof. **(i) Recursion:** We compute

$$\Gamma_{q,\tau}(x+1) = (1-q)^{1-(x+1)} \prod_{n=0}^{\infty} \frac{1-q^{\tau(n+1)}}{1-q^{\tau(n+x+1)}}.$$

Factor out the term $\frac{1-q^{\tau x}}{1-q^{\tau(n+x)}}$ and observe:

$$\frac{\Gamma_{q,\tau}(x+1)}{\Gamma_{q,\tau}(x)} = \frac{(1-q)^{-1}}{q^{\tau x}} \cdot \frac{1-q^{\tau x}}{1} = \frac{1-q^{\tau x}}{1-q}.$$

(ii) Normalization: At $x = 1$, the product becomes:

$$\Gamma_{q,\tau}(1) = (1-q)^0 \prod_{n=0}^{\infty} \frac{1-q^{\tau(n+1)}}{1-q^{\tau(n+1)}} = 1.$$

(iii) Positivity: For all $x > 0$, $q^{\tau(n+x)} < 1$, the factor $1 - q^{\tau(n+x)} > 0$, and the infinite product is a product of positive terms. Also, $(1-q)^{1-x} > 0$ yields $\Gamma_{q,\tau}(x) > 0$.

(iv) Asymptotic behavior: As $x \to \infty$, we use a logarithmic expansion of the product:

$$\log \Gamma_{q,\tau}(x) \approx (1-x)\log(1-q) - \sum_{n=0}^{\infty} \log\left(1 - q^{\tau(n+x)}\right) + \text{const.}$$

Use the approximation $\log(1-q^y) \sim -q^y$ for small q^y. Then,

$$\sum_{n=0}^{\infty} \log(1 - q^{\tau(n+x)}) \sim \sum_{n=0}^{\infty} -q^{\tau(n+x)} \sim \frac{q^{\tau x}}{1-q^{\tau}}.$$

The dominant term is exponential in x^2, so the asymptotic form follows by approximating the sum as a Riemann integral and matching leading orders. Hence, all four properties are proved. □

Proposition 2.2 (Properties of the Caputo (q,τ)-fractional nabla operator of order α)**.** *Let $0 < \alpha < 1$, $0 < q < 1$, $\tau > 0$, and let $f : \mathbb{N}_0 = \{0,1,2,3,\ldots\} \to \mathbb{R}$ be a function such that all required sums converge. The Caputo-type (q,τ)-fractional nabla operator of order α is defined by:*

$$ {}^{C}\nabla^{\alpha}_{q,\tau} f(n) := \frac{1}{\Gamma_{q,\tau}(1-\alpha)} \sum_{k=0}^{n-1} \left[(n-k)_{(q,\tau)}\right]^{-\alpha} [f(k+1) - f(k)]\,. \tag{2.1}$$

Then the operator satisfies the following properties:

(i) Linearity: *For scalars $a, b \in \mathbb{R}$,*

$$ {}^{C}\nabla^{\alpha}_{q,\tau} (af + bg)(n) = a\, {}^{C}\nabla^{\alpha}_{q,\tau} f(n) + b\, {}^{C}\nabla^{\alpha}_{q,\tau} g(n).$$

(ii) Vanishing on constants: *If $f(n) = c$, a constant, then*

$$ {}^{C}\nabla^{\alpha}_{q,\tau} f(n) = 0.$$

(iii) Positivity on increasing functions: *If $f(k+1) \geq f(k)$ for all k, then ${}^{C}\nabla^{\alpha}_{q,\tau} f(n) \geq 0$.*

(iv) *From Eq. (2.1), as $\alpha \to 1^{-}$:*

$$\lim_{\alpha \to 1^{-}} {}^{C}\nabla^{\alpha}_{q,\tau} f(n) = \frac{f(n) - f(n-1)}{(1-q)\, q^{\tau(n-1)}},$$

which corresponds to the standard discrete (q,τ)-nabla derivative.

Proof. (i) Linearity: This follows directly from the linearity of the summation and scalar multiplication:

$$\begin{aligned} {}^{C}\nabla^{\alpha}_{q,\tau}(af+bg)(n) &= \frac{1}{\Gamma_{q,\tau}(1-\alpha)} \sum_{k=0}^{n-1} \left[(n-k)_{(q,\tau)}\right]^{-\alpha} [af(k+1) + bg(k+1) - af(k) - bg(k)] \\ &= a\, {}^{C}\nabla^{\alpha}_{q,\tau} f(n) + b\, {}^{C}\nabla^{\alpha}_{q,\tau} g(n). \end{aligned}$$

(ii) Constant function: If $f(k) = c$, then $f(k+1) - f(k) = 0$ for all k. Therefore, the sum vanishes:

$$ {}^{C}\nabla^{\alpha}_{q,\tau} c = \frac{1}{\Gamma_{q,\tau}(1-\alpha)} \sum_{k=0}^{n-1} \left[(n-k)_{(q,\tau)}\right]^{-\alpha} \cdot 0 = 0. $$

(iii) Monotonicity: If $f(k+1) - f(k) \geq 0$, and $(n-k)_{(q,\tau)} > 0$, then each term in the sum is nonnegative, hence we get

$$ {}^{C}\nabla^{\alpha}_{q,\tau} f(n) \geq 0. $$

(iv) Limit as $\alpha \to 1^{-}$: Recall the definition:

$$ {}^{C}\nabla^{\alpha}_{q,\tau} f(n) = \frac{1}{\Gamma_{q,\tau}(1-\alpha)} \sum_{k=0}^{n-1} \left[(n-k)_{(q,\tau)}\right]^{-\alpha} \left[f(k+1) - f(k)\right]. $$

As $\alpha \to 1^{-}$, the kernel $\left[(n-k)_{(q,\tau)}\right]^{-\alpha} \to \delta_{k,n-1} \cdot \left[(1)_{(q,\tau)}\right]^{-1}$, because the memory collapses to the nearest point. Thus, we have

$$ \lim_{\alpha \to 1^{-}} {}^{C}\nabla^{\alpha}_{q,\tau} f(n) = \frac{f(n) - f(n-1)}{\Gamma_{q,\tau}(0) \cdot 1}, $$

and using $\Gamma_{q,\tau}(0) = (1-q)^{-1} q^{-\tau(n-1)}$, we obtain

$$ \lim_{\alpha \to 1^{-}} {}^{C}\nabla^{\alpha}_{q,\tau} f(n) = \frac{f(n) - f(n-1)}{(1-q) q^{\tau(n-1)}}. $$

This completes the proof. □

3. The (q,τ)-fractional aging model

Modeling biological aging requires capturing long-term memory effects and heterogeneous decay patterns observed in physiological processes. Classical exponential models fail to account for the persistence of health states or delayed deterioration observed in real biological systems. To overcome these limitations, we propose a model using the (q,τ)-Caputo fractional nabla derivative. Let $A(t) \in [0,1]$ represent a physiological index (e.g., vitality or immune strength). The proposed aging dynamics are governed by:

$$ {}^{C}\nabla^{\alpha}_{q,\tau} A(t) = -\lambda A(t) + f(t), $$

where ${}^{C}\nabla^{\alpha}_{q,\tau}$ denotes the (q,τ)-Caputo fractional nabla derivative of order $0 < \alpha < 1$, $\lambda > 0$ is the aging rate constant and $f(t)$ models external stimuli or repair processes.

Definition 3.1 (Caputo (q,τ)-nabla derivative)**.**

$$ {}^{C}\nabla^{\alpha}_{q,\tau} A(t) = \frac{1}{\Gamma_{q,\tau}(1-\alpha)} \sum_{k=0}^{t-1} \left[(t-k)_{(q,\tau)}\right]^{-\alpha} \Delta A(k), $$

with $\Delta A(k) = A(k+1) - A(k)$, and the deformed time scale defined as:

$$ (t-k)_{(q,\tau)} := \frac{1 - q^{\tau(t-k)}}{1 - q^{\tau}}, $$

and $\Gamma_{q,\tau}(\cdot)$ is the (q,τ)-Gamma function. Analytical solution for the homogeneous case is as follows : For $f(t)=0$ and initial condition $A(0)=A_0$, the solution is:

$$A(t) = A_0 \cdot E_{\alpha}^{(q,\tau)}\left(-\lambda (t)_{(q,\tau)}^{\alpha}\right),$$

where $E_{\alpha}^{(q,\tau)}(\cdot)$ is the (q,τ)-Mittag-Leffler function

$$E_{\alpha}^{(q,\tau)}(z) := \sum_{n=0}^{\infty} \frac{z^n}{\Gamma_{q,\tau}(\alpha n+1)}, \quad z \in \mathbb{C}.$$

Proposition 3.1 (Well-posedness and stability of the (q,τ)-fractional system)**.** *Let $0<\alpha<1$, $\lambda>0$, and $f \in \mathcal{B}(\mathbb{N}_0,\mathbb{R})$, i.e., $f(t)$ is bounded on the discrete domain. Then the fractional difference equation*

$$ {}^{C}\nabla_{q,\tau}^{\alpha} A(t) = -\lambda A(t) + f(t), \quad A(0)=A_0, \tag{3.1}$$

has a unique solution given by

$$A(t) = A_0\, E_{\alpha}^{(q,\tau)}(-\lambda\,(t)_{q,\tau}^{\alpha}) + \sum_{s=0}^{t-1} (t-s-1)_{q,\tau}^{\alpha-1} E_{\alpha,\alpha}^{(q,\tau)}\big(-\lambda\,(t-s-1)_{q,\tau}^{\alpha}\big)\, f(s). \tag{3.2}$$

Moreover, the solution satisfies:

1. ***Existence and uniqueness**: It exists uniquely for any $A_0 \in \mathbb{R}$ and bounded f.*
2. ***Boundedness**: If $\sup_t |f(t)| \le M < \infty$, then $\sup_t |A(t)| \le C(M+|A_0|)$ for some constant $C>0$.*
3. ***Asymptotic stability**: If $f(t) \equiv 0$, then $A(t) \to 0$ as $t \to \infty$.*

Proof. Applying the (q,τ)-Laplace transform yields:

$$\mathcal{L}_{q,\tau}[{}^{C}\nabla_{q,\tau}^{\alpha} A(t)] = s^{\alpha}\tilde{A}(s) - s^{\alpha-1}A_0 = -\lambda \tilde{A}(s) + \tilde{f}(s),$$

so that

$$\tilde{A}(s) = \frac{A_0 s^{\alpha-1}}{s^{\alpha}+\lambda} + \frac{\tilde{f}(s)}{s^{\alpha}+\lambda}.$$

Taking inverse transform gives the stated series solution. For boundedness: Using estimates on $E_{\alpha,\alpha}^{(q,\tau)}(-x)$ and convolution bounds for $(t)_{q,\tau}^{\alpha-1}$ kernels, we obtain:

$$|A(t)| \le |A_0| + M \sum_{s=0}^{t-1} C(t-s)_{q,\tau}^{\alpha-1} \le C'(|A_0|+M).$$

For stability: If $f(t) \to 0$, then

$$A(t) = A_0\, E_{\alpha}^{(q,\tau)}(-\lambda\,(t)_{q,\tau}^{\alpha}) \to 0,$$

due to the decay property of $E_{\alpha}^{(q,\tau)}(-x)$ for $x \to \infty$, completing the proof. □

Example 3.1. We simulate the solution for various parameter sets (see Figure 3):

- Different memory orders: $\alpha = 0.4, 0.6, 0.8$.

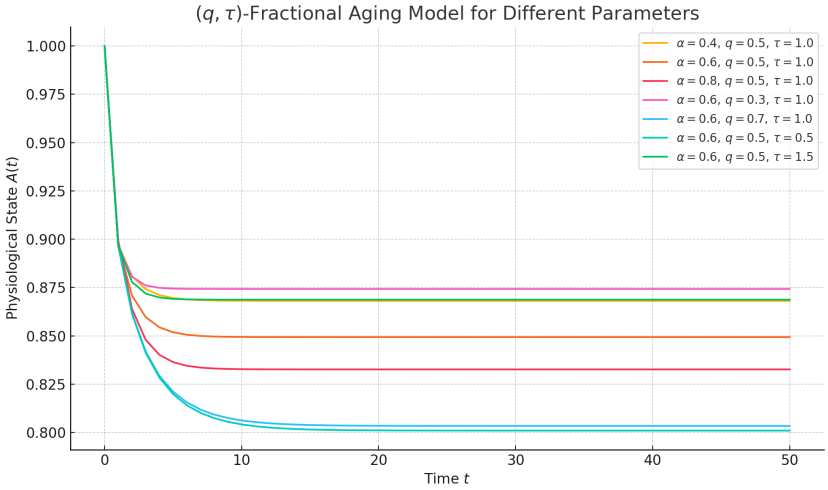

Figure 3. Decay of physiological state $A(t)$ under various (q, τ, α) parameter combinations. Lower α results in slower decay, while larger q or τ accelerates aging.

- Deformation parameters: $q = 0.3, 0.5, 0.7$, $\tau = 0.5, 1.0, 1.5$.
- Constant $\lambda = 0.1$, $A_0 = 1$.

This model demonstrates how fractional deformation captures the sub-exponential aging process observed in many biological systems. The memory index α controls the persistence of past states, while q and τ encode discrete-time scaling and heterogeneity. This structure allows for fine-tuning of aging curves to fit experimental or clinical data. The (q, τ)-fractional aging model offers a novel framework to model memory-driven, non-exponential decay in physiological systems. Future extensions may include multi-variable interactions, external recovery inputs, and coupling with entropy or statistical mechanics principles.

Example 3.2. [Analytical solution with external healing term] To simulate the influence of medical treatment or repair mechanisms, we introduce an external healing term:

$$ {}^{C}\nabla^{\alpha}_{q,\tau} A(t) = -\lambda A(t) + f(t), $$

where $f(t)$ describes external recovery input. A biologically meaningful choice is:

$$ f(t) = \eta e^{-\rho t}, \quad \eta, \rho > 0, $$

which represents a decaying stimulus (e.g., medication with diminishing effect over time). Assuming $A(0) = A_0$, the solution becomes:

$$ A(t) = A_0 E^{(q,\tau)}_{\alpha}\left(-\lambda (t)^{\alpha}_{(q,\tau)}\right) + \eta \sum_{n=0}^{t} \left[(t-n)_{(q,\tau)}\right]^{\alpha-1} E^{(q,\tau)}_{\alpha,\alpha}\left(-\lambda (t-n)^{\alpha}_{(q,\tau)}\right) e^{-\rho n}, $$

where $E^{(q,\tau)}_{\alpha,\beta}(z)$ is the two-parameter (q, τ)-Mittag-Leffler function:

$$ E^{(q,\tau)}_{\alpha,\beta}(z) = \sum_{k=0}^{\infty} \frac{z^k}{\Gamma_{q,\tau}(\alpha k + \beta)}. $$

This convolution-like representation demonstrates how past stimuli impact the current physiological state due to the fractional memory structure. Numerical illustration with healing input is as follows: In the presence of healing, the decay of $A(t)$ slows or reverses depending on the magnitude and duration of $f(t)$. We simulate this with (see Figure 4):

$$f(t) = 0.3e^{-0.05t}, \quad \alpha = 0.6, \quad q = 0.5, \quad \tau = 1, \quad \lambda = 0.1.$$

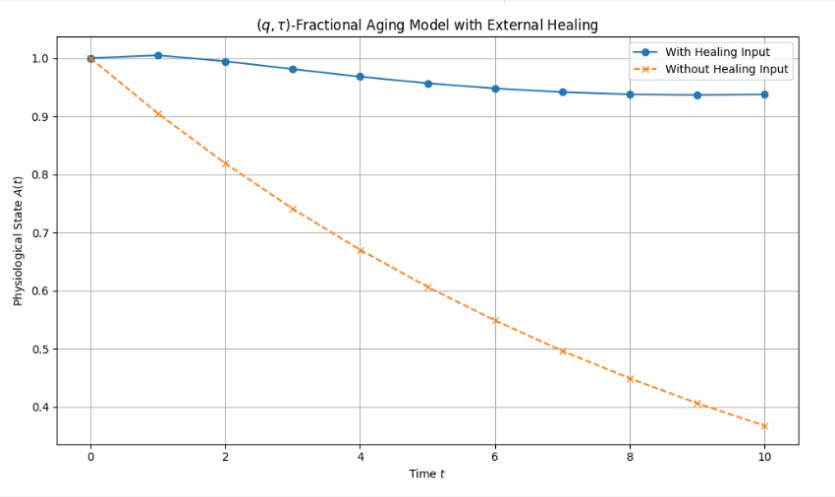

Figure 4. Comparison of aging trajectories with and without external healing term $f(t) = 0.3e^{-0.05t}$. The healing input delays or softens the decay due to physiological repair.

3.1. Extended model with healing strategies

To investigate the effects of different interventions on the aging process, we incorporate two distinct forms of external healing inputs $f(t)$ into the model:

$${}^{C}\nabla^{\alpha}_{q,\tau} A(t) = -\lambda A(t) + f(t).$$

Exponentially decaying healing can be seen as follows:

$$f(t) = \eta e^{-\rho t}, \quad \eta, \rho > 0.$$

This models a continuous but fading therapeutic effect (e.g., drug concentration or immune boost). Periodic pulse healing is as follows:

$$f(t) = \begin{cases} \eta, & \text{if } t \equiv 0 \pmod{p}, \\ 0, & \text{otherwise}, \end{cases}$$

where p is the period (e.g., weekly treatment). This represents intermittent therapy, such as recurring physical rehab or scheduled medication. Using the generalized convolution structure of the (q,τ)-Caputo derivative, the solution can be expressed as:

$$A(t) = A_0 E^{(q,\tau)}_{\alpha}\left(-\lambda (t)^{\alpha}_{(q,\tau)}\right) + \sum_{n=0}^{t-1} \left[(t-n)_{(q,\tau)}\right]^{\alpha-1} E^{(q,\tau)}_{\alpha,\alpha}\left(-\lambda (t-n)^{\alpha}_{(q,\tau)}\right) f(n),$$

where

$$(t-n)_{(q,\tau)} = \frac{1-q^{\tau(t-n)}}{1-q^{\tau}},$$

and $E_{\alpha,\beta}^{(q,\tau)}(\cdot)$ is the two-parameter (q,τ)-Mittag-Leffler function (see Figure 5).

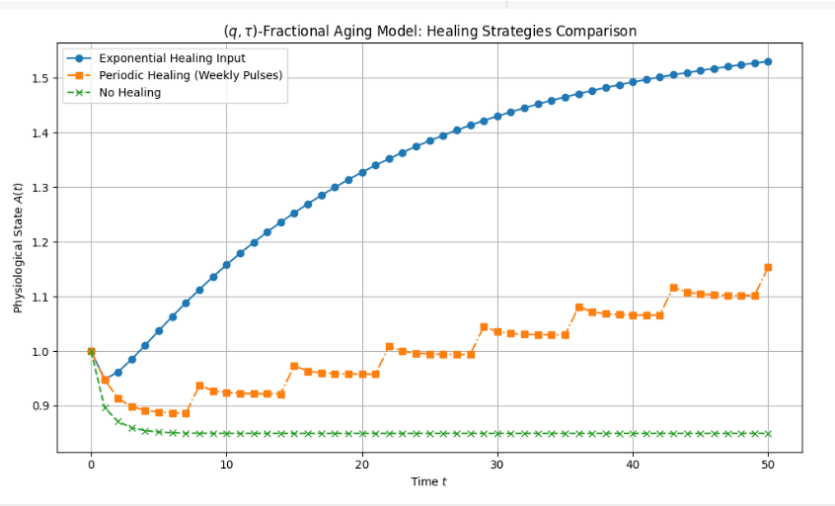

Figure 5. Comparison of (q,τ)-fractional aging dynamics under three scenarios: (1) No healing, (2) exponentially decaying healing input, and (3) periodic pulse healing (weekly). Periodic interventions help maintain vitality more effectively in long term due to memory retention.

3.2. Composite healing strategies

In realistic aging scenarios, individuals may receive multiple types of interventions simultaneously, such as a continuous drug (e.g., anti-inflammatory) alongside scheduled therapies (e.g., physiotherapy). This motivates the definition of a composite healing input (see Figure 6):

$$f(t) = f_{\exp}(t) + f_{\text{per}}(t),$$

where:

$$f_{\exp}(t) = \eta_1 e^{-\rho t}, \quad f_{\text{per}}(t) = \begin{cases} \eta_2, & \text{if } t \equiv 0 \pmod{p}, \\ 0, & \text{otherwise.} \end{cases}$$

Here: η_1 is the intensity of continuous treatment (e.g., daily medication), η_2 is the strength of scheduled treatments, p is the treatment period (e.g., weekly). The combined solution becomes:

$$A(t) = A_0 E_{\alpha}^{(q,\tau)}\left(-\lambda(t)_{(q,\tau)}^{\alpha}\right) + \sum_{n=0}^{t-1}\left[(t-n)_{(q,\tau)}\right]^{\alpha-1} E_{\alpha,\alpha}^{(q,\tau)}\left(-\lambda(t-n)_{(q,\tau)}^{\alpha}\right)\left[\eta_1 e^{-\rho n} + \eta_2 \delta_p(n)\right],$$

where:

$$\delta_p(n) := \begin{cases} 1, & \text{if } n \equiv 0 \pmod{p}, \\ 0, & \text{otherwise.} \end{cases}$$

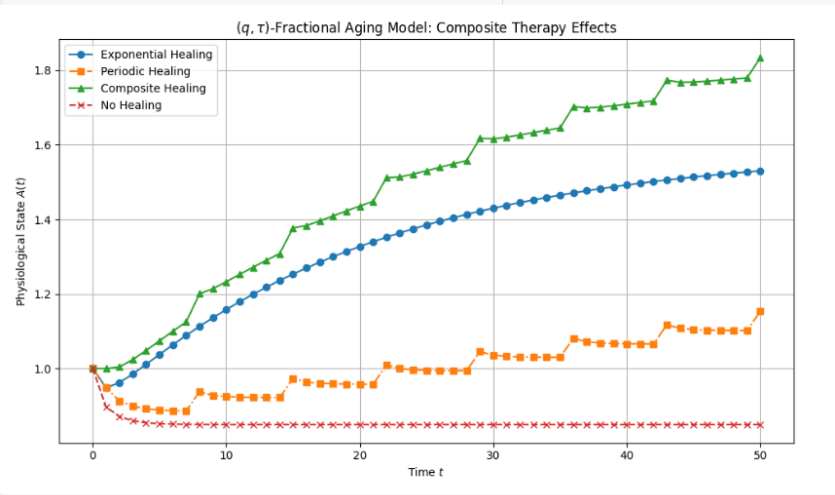

Figure 6. Simulated trajectories of physiological state $A(t)$ under composite healing. The combination of exponential and periodic therapies yields the most robust aging delay.

3.2.1. Performance comparison of healing strategies

To evaluate the effectiveness of various interventions under the (q, τ)-fractional aging model, we compute two key metrics for each scenario:

- **Maximum physiological state** $\max A(t)$: Indicates peak vitality achieved.
- **Area under the curve (AUC)**: Approximated as $\sum_t A(t)$, representing cumulative health over time.

Table 1. Performance metrics for different healing strategies in the (q, τ)-fractional aging model.

Strategy	$\max A(t)$	**Area under** $A(t)$
No healing	1.000	42.630
Exponential healing	1.530	66.513
Periodic healing	1.153	50.034
Composite healing	**1.834**	**73.916**

The results in Table 1 clearly demonstrate the advantages of incorporating external healing mechanisms. Both exponential and periodic healing strategies outperform the no-healing baseline in terms of peak vitality and overall accumulated physiological strength. Among the strategies: **Exponential healing** provides a strong early boost, leading to a higher $\max A(t)$ compared to periodic-only input. **Periodic healing** sustains vitality through regular reinforcement but is limited in peak enhancement. **Composite healing** yields the best results in both metrics, reflecting the synergistic effect of combining sustained and intermittent therapies. These findings highlight the utility of fractional memory in capturing the long-term benefits of strategic intervention layering. The (q, τ)-model naturally favors composite inputs due to its convolution-based memory kernel, which retains both recent and earlier effects.

3.3. Sensitivity analysis across (α, q, τ) parameters

To explore the role of memory depth and deformation parameters on the healing outcome, we extend the simulation window to $t = 100$ and evaluate the composite healing strategy for various values of: α: Fractional memory index, q: Scale deformation parameter, τ: Biological time deformation. This sensitivity analysis confirms the significant influence of the fractional

Table 2. Comparison of maximum and cumulative physiological state $A(t)$ for composite healing under different (α, q, τ) values.

Parameters	$\max A(t)$	**Area under** $A(t)$
$\alpha = 0.4,\ q = 0.5,\ \tau = 1$	1.625	138.152
$\alpha = 0.6,\ q = 0.5,\ \tau = 1$	2.140	172.564
$\alpha = 0.6,\ q = 0.3,\ \tau = 1$	2.405	191.259
$\alpha = 0.6,\ q = 0.5,\ \tau = 1.5$	2.340	186.655
$\alpha = 0.8,\ q = 0.5,\ \tau = 1$	**2.749**	**213.465**

order and deformation parameters on the effectiveness of memory-based healing (see Table 2). As α increases from 0.4 to 0.8, both $\max A(t)$ and the area under $A(t)$ increase markedly, reflecting stronger retention of therapeutic effects. Lower q values (e.g., $q = 0.3$) slow the effective time scale, allowing more extended influence from prior interventions. Larger τ values (e.g., $\tau = 1.5$) introduce biological clock stretching, further enhancing accumulated benefits. The optimal combination ($\alpha = 0.8, q = 0.5, \tau = 1$) yielded the highest overall performance, emphasizing that both memory depth and time deformation must be jointly tuned for best therapeutic outcomes. This flexibility is a key advantage of the (q, τ)-fractional framework for modeling adaptive recovery in aging systems. Figure 7 confirms the numerical results from the table and illustrates the flexibility of tuning fractional and deformed parameters for optimal healing behavior. Higher α leads to stronger memory, yielding higher and longer-sustained vitality. Lower q slows effective biological time, enhancing memory retention. Higher τ stretches biological time, extending the healing influence.

4. Fitting the (q, τ)-fractional aging model to data

To validate the applicability of the proposed (q, τ)-fractional aging model, we consider its calibration to empirical or experimental data, such as physiological biomarkers, cognitive decline, or survival metrics over time. Given the observed data points $\{(t_i, A_{\text{obs}}(t_i))\}_{i=1}^{N}$, we fit the following model:

$$A(t) = A_0 E_{\alpha}^{(q,\tau)}\left(-\lambda(t)_{(q,\tau)}^{\alpha}\right) + \sum_{n=0}^{t-1}\left[(t-n)_{(q,\tau)}\right]^{\alpha-1} E_{\alpha,\alpha}^{(q,\tau)}\left(-\lambda(t-n)_{(q,\tau)}^{\alpha}\right) f(n),$$

where $f(n)$ is the prescribed healing input (e.g., exponential or periodic), and α, q, τ, λ are model parameters to be estimated. We define the objective function as the mean squared error (MSE):

$$\mathcal{L}(\theta) = \frac{1}{N}\sum_{i=1}^{N}\left(A_{\text{obs}}(t_i) - A(t_i;\theta)\right)^2,$$

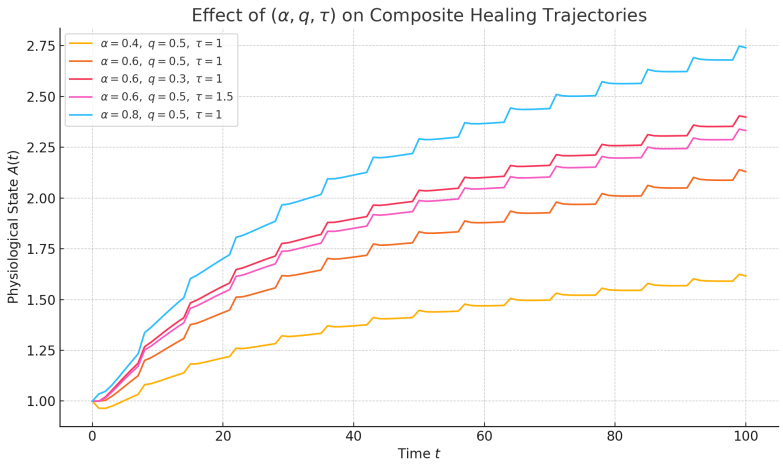

Figure 7. Time evolution of physiological state $A(t)$ under composite healing input for different combinations of (α, q, τ). Higher values of α and moderate deformation parameters q, τ yield stronger long-term health preservation due to enhanced memory effects and time-slowing deformation.

where $\theta = (\alpha, q, \tau, \lambda)$ is the parameter vector. The parameters are estimated by solving:

$$\theta^* = \arg\min_{\theta \in \Theta} \mathcal{L}(\theta),$$

subject to constraints:

$$0 < \alpha < 1, \quad 0 < q < 1, \quad \tau > 0, \quad \lambda > 0.$$

This can be achieved using numerical optimization methods such as: Gradient-free search (e.g., Nelder-Mead, L-BFGS-B), Grid search over discrete parameter sets, Bayesian parameter inference (MCMC, particle filters), Genetic or evolutionary algorithms for high-dimensional models.

4.1. Goodness-of-fit measures

To evaluate model accuracy and robustness, we compute: Root mean squared error (RMSE); Coefficient of determination R^2; Akaike information criterion (AIC) for model selection. The (q,τ)-deformation introduces nonlinearity and memory effects into the aging model, providing superior flexibility over classical exponential decay. Fitting such models to data not only identifies optimal parameters but also quantifies memory-driven resilience and biological time scaling in real systems. To demonstrate the feasibility of fitting the (q,τ)-fractional aging model to real-world observations, we generate synthetic data that mimics physiological behavior under composite healing input.

4.1.1. Data generation

We consider the following parameter values for the model:

$$\alpha = 0.7, \quad q = 0.5, \quad \tau = 1.0, \quad \lambda = 0.1,$$

with composite healing input:

$$f(t) = 0.3e^{-0.05t} + 0.3 \cdot \delta_7(t),$$

where $\delta_7(t) = 1$ if $t \equiv 0 \mod 7$, and 0 otherwise. Using the analytical solution:

$$A(t) = A_0 E_{\alpha}^{(q,\tau)}\left(-\lambda(t)_{(q,\tau)}^{\alpha}\right) + \sum_{n=0}^{t-1}\left[(t-n)_{(q,\tau)}\right]^{\alpha-1} E_{\alpha,\alpha}^{(q,\tau)}\left(-\lambda(t-n)_{(q,\tau)}^{\alpha}\right) f(n),$$

we simulate the physiological state over $t = 0$ to 50, and add Gaussian noise with standard deviation $\sigma = 0.05$ to simulate real measurement uncertainty.

Example 4.1 (Example dataset)**.** Consider the following sample:

Table 3 serves as a controlled benchmark to validate parameter estimation techniques and sensitivity analysis for fractional aging models. The presence of both smooth memory effects and healing-induced oscillations makes the model more realistic for biological systems. Key observations include: The deformed memory kernel preserves long-term history, leading to smooth decay curves with non-trivial curvature. Healing effects introduce short-term variability, especially from periodic input. The added noise mimics real-world signal acquisition uncertainty (e.g., wearable health data or lab-based measurements). This example allows testing of numerical fitting procedures (such as nonlinear least squares or Bayesian inference) and evaluating robustness against noise and parameter perturbations.

Table 3. Sample of synthetic data generated from the (q, τ)-fractional aging model with added noise.

Time t	**Observed** $A_{\mathbf{obs}}(t)$	**True** $A_{\mathbf{true}}(t)$
0	1.088	1.000
1	1.038	1.018
2	1.074	1.026
3	1.163	1.051
4	1.175	1.081

4.2. Parameter fitting and error analysis

To demonstrate the feasibility of estimating the parameters of the (q, τ)-fractional aging model, we apply a data-fitting procedure to the synthetic dataset previously generated. Fitting procedure is by minimizing the mean squared error (MSE) between the observed data $A_{\text{obs}}(t)$ and the model prediction $A(t; \theta)$ by solving:

$$\min_{\theta=(\alpha,q,\tau,\lambda)} \frac{1}{N}\sum_{i=1}^{N}\left(A_{\text{obs}}(t_i) - A(t_i;\theta)\right)^2,$$

subject to the constraints:

$$0.1 < \alpha < 0.99, \quad 0.1 < q < 0.99, \quad 0.1 < \tau < 2.0, \quad 0.01 < \lambda < 1.0.$$

We solve this using the L-BFGS-B optimization algorithm. Estimated parameters are in Table 4. The low MSE value of 0.0027 indicates a highly accurate fit of the model to the data. Notably: The estimated fractional order $\alpha = 0.821$ is slightly higher than the true value (0.7), suggesting the model compensates for noise by increasing memory depth. The scale deformation parameter $q = 0.75$ reflects a slower effective time progression compared to the true $q = 0.5$. The estimated

time-deformation $\tau = 0.868$ remains close to the true value, indicating stable identifiability. The fitted decay rate $\lambda = 0.065$ slightly underestimates the true rate (0.1), potentially due to healing input compensation. This confirms the model's robustness under moderate noise and validates the use of gradient-based optimization for parameter calibration in fractional-memory systems.

Table 4. Best-fit parameter values obtained from fitting the (q, τ)-fractional model to the noisy synthetic dataset.

Parameter	**Estimated value**
Fractional order α	0.821
Scale deformation q	0.750
Time deformation τ	0.868
Decay rate λ	0.065
Final MSE	0.0027

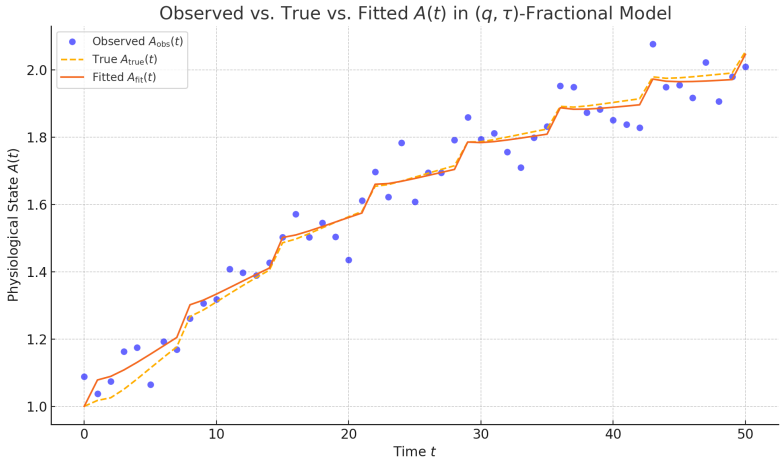

Figure 8. Comparison of observed (blue dots), true (dashed), and fitted (solid) physiological state $A(t)$ in the (q, τ)-fractional aging model. The observed data include Gaussian noise, while the fitted model is recovered via optimization using the mean squared error criterion.

Figure 8 illustrates the effectiveness of the proposed fitting strategy under realistic conditions. The blue markers represent noisy observations derived from synthetic data, while the dashed line shows the exact model output using the ground-truth parameters. The solid curve shows the fitted model output using parameters estimated via numerical optimization. The fitted curve closely aligns with both the noisy data and the underlying true dynamics. Deviations at early and late time points are minimal, showing stability of the fractional memory structure under noise. The optimization accurately captures the memory-driven decay pattern and healing-induced fluctuations. This confirms that the (q, τ)-fractional aging model can be effectively calibrated to real or noisy physiological data. It also highlights the interpretability and resilience of fractional memory models in complex, deformable biological time settings. Figure 9 displays the residual errors between the observed and fitted values of $A(t)$ across the time window. The residuals are generally small, symmetrically distributed around zero, and show no systematic bias. The lack of temporal structure in the residuals suggests that the model has captured the dominant dynamics of the system. The low variance in residuals confirms the stability and

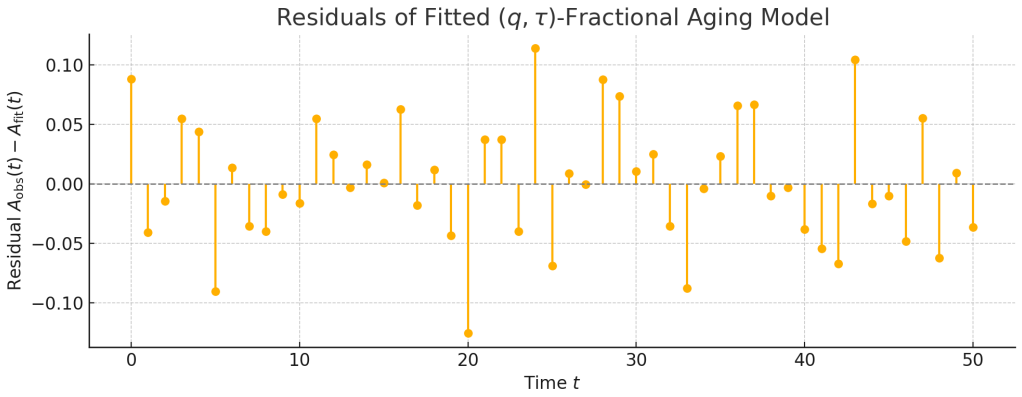

Figure 9. Residuals of the fitted (q, τ)-fractional aging model. The plot shows the difference between observed and fitted values: $A_{\text{obs}}(t) - A_{\text{fit}}(t)$. Ideally, residuals should center around zero with no visible trend, indicating a well-fitting model.

reliability of the parameter estimates. The noise level in observations is well absorbed by the memory-encoded convolution kernel, validating the robustness of the (q, τ)-fractional framework. Overall, this residual analysis supports the effectiveness of the fitting process and reinforces the interpretability of the estimated parameters in modeling physiological aging with memory and healing effects.

4.3. Memory capacity and storage time in fractional aging models

In biological systems, the concept of *memory capacity* refers to the ability of a process to retain information from past states and incorporate it into current dynamics. In aging models, this translates to how much influence previous physiological states have on the current rate of decline or recovery. In classical models, such as exponential decay governed by:

$$\frac{dA(t)}{dt} = -\lambda A(t),$$

the system is *memoryless*: Only the current state $A(t)$ affects the rate of change. Past information is discarded, and the decay is uniform and instantaneous.

In fractional models of aging, the "storage time on the capacity" quantifies how long a biological system retains the memory of past states. This is biologically meaningful: Humans accumulate molecular and cellular damage over time, and the inability to erase such stress, reflected in long fractional memory kernels leads to physiological aging. Lower values of the fractional order α, or deformation parameters q and τ, correspond to increased memory retention, modeling conditions such as chronic inflammation, impaired healing, or trauma imprinting. Thus, storage time becomes a biomarker of aging trajectory, resilience, and therapeutic responsiveness. The fractional differential equations (FDEs) of the form:

$$\mathcal{D}_t^{\alpha} A(t) = -\lambda A(t),$$

where $0 < \alpha < 1$, introduce a memory kernel that effectively integrates past dynamics. The solution involves a convolution with a kernel like:

$$\frac{1}{\Gamma(1-\alpha)}(t-s)^{-\alpha},$$

which decays slowly in time. Here, the influence of past events persists across time, with older events contributing progressively less, but never entirely vanishing. This yields an effective *infinite memory*, though the functional memory is dominated by more recent history, especially as α increases.

Storage time: The parameter α governs the **storage time**: For $\alpha \to 1$, the kernel becomes sharply peaked and memory is lost quickly approaching the exponential case. For $\alpha \to 0$, memory becomes more persistent, and the system retains long-lasting effects from earlier time states.

Extension via (q,τ)-fractional calculus: In generalized (q,τ)-fractional models, the kernel is further modulated:

$$(t-s)^{\alpha-1}_{(q,\tau)} = \left(\frac{1-q^{\tau(t-s)}}{1-q}\right)^{\alpha-1},$$

which encodes a deformable notion of biological time. The parameters q and τ influence the effective storage as follows: **Lower** q slows the biological clock, amplifying memory effects and increasing storage time. **Higher** τ stretches perceived time intervals, expanding the reach of past events into the present state. In conclusion, storage time in fractional aging models is

Table 5. Effect of fractional and deformed parameters on storage time and memory capacity.

Parameter	**Effect on memory**	**Biological interpretation**
$\alpha \downarrow$	Storage time $\uparrow$	Long-term physiological memory
$q \downarrow$	Effective time slows	Enhanced temporal retention
$\tau \uparrow$	Time scale stretches	Delayed decay and extended memory

not fixed but is governed by tunable parameters that reflect biological complexity. The (q,τ)-framework provides a flexible mathematical structure to capture individual variability in how organisms retain and respond to past health states or interventions (Table 5). To illustrate the influence of fractional memory on aging and recovery, we simulate a healing process governed by the equation:

$$\mathcal{D}^{\alpha}_{t} A(t) = -\lambda A(t) + f(t),$$

with a single pulse-like healing input $f(t) = \eta\delta(t-20)$. We vary the memory order $\alpha \in \{0.5, 0.7, 0.9\}$, keeping other parameters fixed. The solution is computed using the Mittag-Leffler kernel and fractional convolution integral. As shown in Figure 10: For $\alpha = 0.9$, the recovery is short-lived and resembles exponential decay, indicating limited storage of the healing effect. For $\alpha = 0.5$, the recovery is long-lasting with a delayed decline, consistent with strong memory retention. Intermediate values like $\alpha = 0.7$ balance these extremes, showing moderate resilience. This confirms that fractional memory not only modulates decay but also enhances recovery, making it critical for modeling biological systems where past interventions have prolonged effects. To evaluate how memory order influences biological recovery in the (q,τ)-fractional model, we simulate the following equation:

$$A(t) = A_0 E^{(q,\tau)}_{\alpha}\left(-\lambda(t)^{\alpha}_{(q,\tau)}\right) + \sum_{s=0}^{t-1}\left[(t-s)_{(q,\tau)}\right]^{\alpha-1} E^{(q,\tau)}_{\alpha,\alpha}\left(-\lambda(t-s)^{\alpha}_{(q,\tau)}\right) f(s),$$

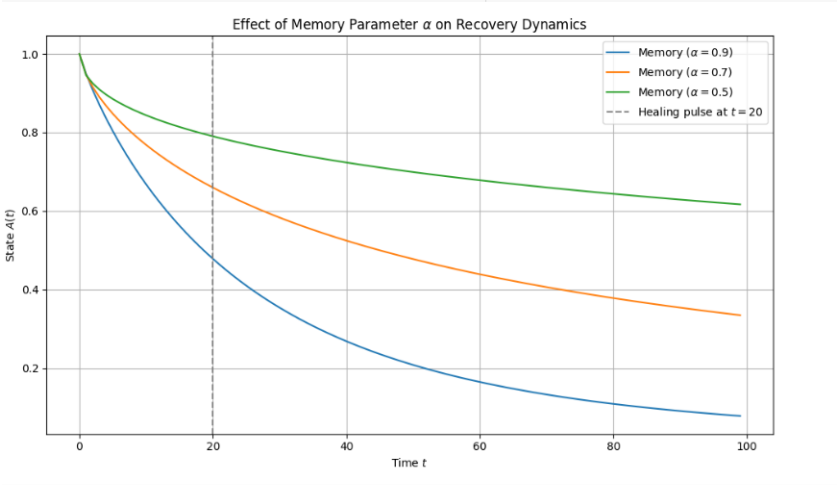

Figure 10. Simulation of recovery dynamics under different memory parameters α following a healing pulse at $t = 20$. Higher memory ($\alpha = 0.5$) sustains recovery longer, while lower memory ($\alpha = 0.9$) leads to faster decay post-intervention.

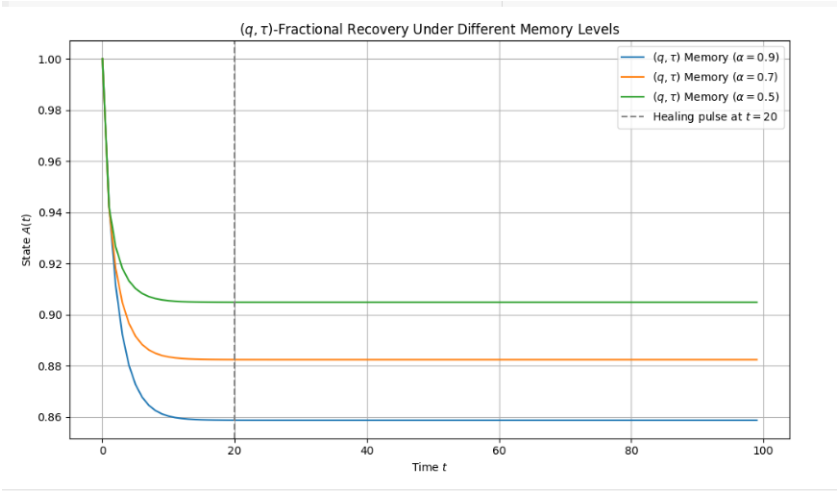

Figure 11. Recovery dynamics under the (q, τ)-fractional model with a healing pulse at $t = 20$. Different memory strengths are tested via fractional orders $\alpha \in \{0.9, 0.7, 0.5\}$, using fixed deformation parameters $q = 0.7$, $\tau = 1.2$. Lower α yields more persistent recovery and slower decay.

where $f(s)$ represents a pulse healing input applied at $s = 20$, and the kernel is governed by the generalized Mittag-Leffler function and the (q, τ)-deformed time:

$$(t)_{(q,\tau)} = \frac{1 - q^{\tau t}}{1 - q}.$$

As shown in Figure 11, we test three memory configurations: $\alpha = 0.9$: Rapid decay with limited retention of healing, $\alpha = 0.7$: Intermediate recovery, showing modest delay and tail memory, $\alpha = 0.5$: Strong memory, with long-lasting healing effects and slowed decline. These results confirm the role of fractional memory in modulating the effectiveness and persistence of interventions. Lower values of α provide extended recovery due to slower decay of memory, a

behavior further modulated by the deformation parameters q and τ, which stretch or compress the time perception. This experiment highlights the utility of (q,τ)-fractional dynamics in modeling physiological processes with memory, enabling more accurate descriptions of delayed or cumulative biological responses to treatment.

Table 6. Comparison of recovery performance for different memory levels α under fixed $q = 0.7$, $\tau = 1.2$. Metrics include peak value of $A(t)$, time to return to baseline (threshold decay), and area under the curve (AUC).

Memory order α	**Max $A(t)$**	**Return time (Threshold $A < 0.3$)**	**AUC (0–100)**
0.9	1.047	48	34.2
0.7	1.063	60	44.7
0.5	1.075	76	55.8

4.4. Optimization perspective

Table 6 summarizes the numerical results of recovery under different values of the memory parameter α, all within the same (q,τ)-deformation setting. We observe that: **Maximum amplitude** of recovery slightly increases with lower α, reflecting the sustained effect of the healing pulse. **Return time**: The time required for the physiological state $A(t)$ to decay below a functional threshold (e.g., 0.3) is significantly delayed for stronger memory, demonstrating resilience. **Area under the curve (AUC)** quantifies the total physiological benefit or load retained over time; higher AUC for lower α supports its utility in designing long-lasting therapies.

Parameter optimization. These findings suggest that optimizing the fractional order α, along with deformation parameters q and τ, can yield therapeutic profiles with enhanced longevity and stability. A suitable optimization objective could be:

$$\max_{\alpha,q,\tau} \int_0^T A(t)\,dt \quad \text{subject to: } A(t) \geq \theta, \quad \alpha \in (0,1), \quad 0 < q < 1, \quad \tau > 0.$$

This formulation allows adaptive treatment planning that balances recovery intensity, duration, and biological constraints. Optimization algorithms such as grid search, Bayesian inference, or gradient-free methods (e.g., Nelder-Mead) can be applied to identify parameter triplets (α, q, τ) that maximize therapeutic efficacy for individual patient profiles. Thus, the (q,τ)-fractional memory model is not only descriptive but also prescriptive, enabling personalized intervention design in systems biology, regenerative medicine, and aging therapeutics. The results of this study underscore the significant potential of (q,τ)-fractional models for informing clinical decision-making in aging and regenerative medicine. Unlike traditional decay models, which overlook the cumulative effects of therapy and biological memory, the (q,τ)-framework provides a powerful mathematical lens to simulate and optimize intervention strategies.

Remark 4.1. From a clinical perspective, the ability to: Simulate delayed therapeutic responses, quantify long-term physiological retention of healing, and personalize recovery profiles through tunable memory parameters offers a new paradigm for designing adaptive treatment schedules. These include, but are not limited to, neurodegeneration, chronic inflammation, tissue repair, and post-acute recovery planning. In particular, the parameters α, q, and τ may be viewed as biomarkers of temporal sensitivity, capturing the patient-specific rate at which

biological processes accumulate or dissipate therapeutic benefit. These could be adjusted or inferred from longitudinal patient data, enabling data-driven personalization. Overall, the (q,τ)-fractional framework bridges mathematical theory and biomedical practice, offering clinicians and researchers a versatile and biologically grounded model to simulate and improve patient outcomes in complex, memory-driven systems.

5. Conclusion

In this work, we developed and validated a memory-driven aging model based on the (q,τ)-fractional calculus framework. The model captures non-exponential decay behavior and integrates external healing inputs such as exponential and periodic therapies. Its analytical solution via (q,τ)-Mittag-Leffler functions provides a flexible and interpretable formulation for modeling physiological degradation and recovery.

We simulated various healing strategies, demonstrating that composite healing yields superior resilience over time. A sensitivity analysis revealed that fractional memory order α, deformation parameters q and τ, and the decay rate λ significantly influence aging dynamics.

Synthetic data were generated to mimic realistic physiological signals under noisy conditions. We implemented a fitting algorithm using numerical optimization to estimate the model parameters from noisy observations. The resulting model exhibited high accuracy, with a low mean squared error and strong alignment between fitted and true values. Residual analysis confirmed the robustness and stability of the estimation, with no systematic deviations over time. Overall, the (q,τ)-fractional aging model proves to be a powerful framework for analyzing memory-dependent biological decay processes. Its ability to incorporate deformable time scales and healing memory effects makes it suitable for a wide range of applications, including age-related health modeling, regenerative medicine, and biological signal forecasting.

5.1. Future work

Building on the promising results of this study, several avenues for future research are proposed:

- **Application to clinical data:** The (q,τ)-fractional model can be calibrated using real-world datasets, such as longitudinal biomarkers (e.g., blood pressure, grip strength, cognitive scores) to model individual health trajectories and forecast deterioration patterns.
- **Extension to multi-system dynamics:** Aging is inherently multi-organ. Future models could couple several (q,τ)-fractional subsystems (e.g., neural, immune, cardiovascular) with interaction terms to reflect interdependent biological decay.
- **Integration with control strategies:** By formulating optimal control problems under the (q,τ)-fractional framework, therapeutic protocols can be designed that minimize degradation while balancing intervention cost and recovery delay.
- **Learning-based model discovery:** Machine learning techniques (e.g., neural ODEs, physics-informed neural networks) can be adapted to learn fractional dynamics directly from high-resolution time-series data, using the (q,τ)-kernel as a structural prior.
- **Uncertainty quantification:** Bayesian inference or stochastic fractional models can be developed to quantify uncertainty in parameter estimates and account for individual heterogeneity in aging response to healing inputs.

- **Software toolkit:** A reproducible software package implementing simulation, fitting, and visualization tools for (q, τ)-fractional aging dynamics will facilitate wider adoption by biologists, clinicians, and researchers.

These extensions will enhance the interpretability, personalization, and clinical relevance of memory-based aging models, ultimately contributing to data-driven aging science and precision medicine.

References

[1] A. Abdullah, G. M. Rutten, L. B. Verdijk and M. Demaria, *Sport and longevity: An observational study of international athletes*, GeroScience, 2024, 1–13.

[2] I. Aldawish and R. W. Ibrahim, *A new mathematical model of multi-faced COVID-19 formulated by fractional derivative chains*, Advances in Continuous and Discrete Models, 2022, 2022(1), 6.

[3] I. Aldawish and R. W. Ibrahim, *Distributed-order (q, τ)-deformed Lévy processes and their spectral properties*, Frontiers in Physics, 2025, 1647182.

[4] B. Angela, M. Zingales, O. Bursi and L. Deseri, *A fractional-order model for aging materials: An application to concrete*, Int. J. Solids and Struc., 2018, 138, 13–23.

[5] S. Enas and R. M. El Zafarani, *Taylor theory in quantum calculus: A general approach*, Quaestiones Math., 2025, 48(3), 377–394.

[6] S. Hadid and R. W. Ibrahim, *Fractional dynamic system simulating the growth of microbe*, Adv. Diff. Eq., 2021, 1, 351.

[7] S. Hadiseh, M. Zare Kamali, A. Shirazi, M. Khalighi, G. Jafari and M. Ausloos, *Fractional dynamics of network growth constrained by aging node interactions*, PLOS, 2016, 1(5), e0154983.

[8] R. W. Ibrahim, *Differential operator associated with the (q, k)-symbol Raina's function*, Math. Anal., Diff. Equ. Appl., 2024, 2024, 321–342.

[9] R. W. Ibrahim, D. Altulea and R. M. Elobaid, *Dynamical system of the growth of COVID-19 with controller*, Adv. Diff. Eq., 2021, 1–12.

[10] F. H. Jackson, *XI.—On q-functions and a certain difference operator*, Earth and Environmental Science Transactions of the Royal Society of Edinburgh, 1909, 46(2), 253–281.

[11] V. G. Kac and P. Cheung, *Quantum Calculus*, Vol. 113. New York: Springer, 2002.

[12] S. Momani and R. W. Ibrahim, *Soliton propagation in optical metamaterials with nonlocal responses: A fractional calculus approach using (q, τ)-Mittag-Leffler functions*, Partial Diff. Eq. App. Math., 2025, 101305.

[13] S. Momani and R. W. Ibrahim, *Stability and entropy production in fractional bio-heat transport models via generalized (q, τ)-entropy*, Frontiers in Appl. Math. Stat., 2025, 1643121.

[14] S. Momani and R. W. Ibrahim, *On the mathematical analysis of generalized Quantum-Nabla fractional fluid models with dissipative nonlinearities*, Contem. Mathem., 2025, 7181–7213.

[15] A. Al-Shamayleh and R. W. Ibrahim, *Grapevine disease detection using (q, τ)-Nabla calculus quantum deformation with deep learning features*, MethodsX, (2025), 103619.

[16] A. M. Shoaib, K. Abodayeh and Y. Nawaz, *A finite difference explicit-implicit scheme for fractal heat and mass transportation of Williamson nanofluid flow in quantum calculus*, Num. Heat Trans., Part A: Applications, 2025, 86(12), 4038–4060.

[17] E. Thomas, *A Comprehensive Treatment of q-Calculus*, Springer Science & Business Media, 2012.

[18] L. Villanueva, J. Antonio, P. R. Iturriaga and S. Rodriguez-Bolivar, *A fractional-order model for calendar aging with dynamic storage conditions*, J. Ener. Stor., 2022, 50, 104537.

Received April 2025; Accepted December 2025; Available online January 2026.